The Astrophysical Journal Letters, 987:L2 (7pp), 2025 July 1 https://doi.org/10.3847/2041-8213/ade393

Dissecting the Massive Pristine, Neutral Gas Reservoir of a Remarkably Bright Galaxy at $z = 14.179$

Kasper E. Heintz[1,2,3], Clara L. Pollock[1,2], Joris Witstok[1,2], Stefano Carniani[4], Kevin N. Hainline[5], Francesco D'Eugenio[6,7], Chamilla Terp[2], Aayush Saxena[8,9], and Darach Watson[1,2]
[1] Cosmic Dawn Center (DAWN), Denmark
[2] Niels Bohr Institute, University of Copenhagen, Jagtvej 128, 2200 Copenhagen N, Denmark
[3] Department of Astronomy, University of Geneva, Chemin Pegasi 51, 1290 Versoix, Switzerland
[4] Scuola Normale Superiore, Piazza dei Cavalieri 7, I-56126 Pisa, Italy
[5] Steward Observatory, University of Arizona, 933 North CherryAvenue, Tucson, AZ 85721, USA
[6] Kavli Institute for Cosmology, University of Cambridge, Madingley Road, Cambridge CB3 0HA, UK
[7] Cavendish Laboratory, University of Cambridge, 19 JJ Thomson Avenue, Cambridge CB3 0HE, UK
[8] Department of Physics, University of Oxford, Denys Wilkinson Building, Keble Road, Oxford OX1 3RH, UK
[9] Department of Physics and Astronomy, University College London, Gower Street, London WC1E 6BT, UK
Received 2025 February 11; revised 2025 May 26; accepted 2025 May 29; published 2025 June 23

Abstract

At cosmic dawn, the first stars and galaxies are believed to form from and be deeply embedded in clouds of dense, pristine gas. Here we present a study of the James Webb Space Telescope/NIRSpec data of the most distant, spectroscopically confirmed galaxy observed to date, JADES-GS-z14-0 (GS-z14 for short), at $z = 14.179$, combined with recently reported far-infrared measurements of the [O III]-88 μm and [C II]-158 μm line transitions and underlying dust-continuum emission. Based on the observed prominent damped Lyα (DLA) absorption profile, we determine a substantial neutral atomic hydrogen (H I) column density, $\log(N_{\rm HI}/{\rm cm}^{-2}) = 22.27^{+0.08}_{-0.09}$, consistent with previous estimates though seemingly at odds with the dynamical and gas mass of the galaxy. Using various independent but complementary approaches, considering the implied neutral gas mass from the DLA measurement, the star formation rate surface density, and the metal abundance, we demonstrate that the total gas mass of GS-z14 is of the order $M_{\rm gas} = 10^{9.5}$–$10^{9.8}\,M_{\odot}$. This implies a substantial gas mass fraction, $f_{\rm gas} \approx 0.7$–0.9 and that the bulk of the interstellar medium (ISM) is in the form of H I, with mass ratios $M_{\rm HI}/M_{\rm H_2} \approx 3$. We show that the derived gas mass is fully consistent with the nondetection of [C II]-158 μm, assuming an appropriate scaling to the neutral gas. The low dust-to-gas ratio, $A_V/N_{\rm HI} = (1.3 \pm 0.6) \times 10^{-23}$ mag cm^2, derived in the line of sight through the DLA further indicates that the absorbing gas is more pristine than the central, star-forming regions probed by the [O III]-88 μm emission. These results highlight the implications for far-infrared line-detection searchers attainable with the Atacama Large Millimeter/submillimeter Array and demonstrate that the bright, relatively massive galaxy GS-z14 at $z = 14.179$ is deeply embedded in a substantial, pristine H I gas reservoir dominating its baryonic matter content.

Unified Astronomy Thesaurus concepts: High-redshift galaxies (734); Galaxy formation (595); Reionization (1383); Primordial galaxies (1293)

1. Introduction

The first stars and galaxies are believed to have formed within the first 150–250 Myr after the Big Bang, at redshifts around $z = 15$–20 (see, e.g., B. E. Robertson 2022 for a review). This process is mainly driven by the inflow of pristine gas, mostly in the form of neutral atomic hydrogen (H I), onto dark matter halos. With the advent of the James Webb Space Telescope (JWST), we are now starting to uncover and spectroscopically characterize a substantial population of galaxies close to this first assembly stage at $z = 10$–14 (P. Arrabal Haro et al. 2023; A. J. Bunker et al. 2023; E. Curtis-Lake et al. 2023; M. Castellano et al. 2024; S. Carniani et al. 2024, 2025; T. Y.-Y. Hsiao et al. 2024a, 2024b; J. Witstok et al. 2025; J. A. Zavala et al. 2025) and potentially even more distant sources at $z > 15$, as indicated by their photometry (e.g., R. P. Naidu et al. 2022; H. Atek et al. 2023; R. J. Bouwens et al. 2023; M. Castellano et al. 2022, 2023; C. T. Donnan et al. 2023; Y. Harikane et al. 2023; D. Austin et al. 2024; V. Kokorev et al. 2025; L. Whitler et al. 2025).

The redshifts for these distant sources can be difficult to accurately pinpoint with JWST near-infrared spectroscopy alone, as the Lyα break redshifts were found already in early JWST data to systematically overestimate the emission-line redshifts (e.g., P. Arrabal Haro et al. 2023; E. Curtis-Lake et al. 2023; S. Fujimoto et al. 2023a; S. L. Finkelstein et al. 2024). This effect was later shown to originate from dense, neutral gas reservoirs in and around these galaxies, some with substantial H I column densities, $N_{\rm HI} \gtrsim 10^{22}$ cm^{-2}, in the form of extremely damped Lyα (DLA) absorption line profiles (K. E. Heintz et al. 2024b; H. Umeda et al. 2023; F. D'Eugenio et al. 2024; K. N. Hainline et al. 2024a; J. Witstok et al. 2025). These deep DLA absorption profiles even systematically bias the photometrically derived redshifts due to their high incidence rate in the overall $z \gtrsim 9$ galaxy population (K. E. Heintz et al. 2025; Y. Asada et al. 2025). These measurements indicate that we are starting to probe the primordial matter that drives the formation of these galaxies and fuels their intense, early star formation activity.

Due to the intrinsic faintness of rest-frame UV emission lines covered by JWST/NIRSpec for galaxies at $z > 10$, and

with the added complication of potential strong DLA absorption, a promising alternative avenue of accurately determining the redshift of these sources is via bright far-infrared emission lines. While the first efforts with the Atacama Large Millimeter/submillimeter Array (ALMA) mostly returned nondetections (S. Fujimoto et al. 2023b), the [O III]-88 μm emission of the galaxy GHZ2 was detected at $z = 12.33$ (J. A. Zavala et al. 2024). Further, ALMA observations of JADES-GS-z14-0 (GS-z14 for short) revealed a significant detection of the [O III]-88 μm line (S. Carniani et al. 2025; S. Schouws et al. 2024), lining up precisely with a marginal (3.6σ) NIRSpec detection of the C III]λ1907, 1909 Å doublet (S. Carniani et al. 2024). The line redshift was thus confirmed to be at $z = 14.1796 \pm 0.0006$, substantially lower ($\Delta z = 0.14$) than the photometric and Lyα break redshifts due to the strong DLA recovered in the JWST spectrum (S. Carniani et al. 2025). Deep ALMA follow-up observations targeting the far-infrared [C II]-158 μm line revealed a nondetection, however, which potentially indicates a surprisingly low gas fraction in GS-z14 (S. Schouws et al. 2025) compared to other high-redshift sources (e.g., K. E. Heintz et al. 2023b; M. Aravena et al. 2024; H. Algera et al. 2025).

In this Letter, we reanalyze the JWST/NIRSpec Prism spectrum of GS-z14 in the context of its H I gas content, corroborated by recent far-infrared line emission and continuum measurements. In Section 2, we detail the observational data, and in Section 3, we present the main analysis and results. In Section 4, we will discuss and conclude on our work. Throughout the Letter, we assume the concordance ΛCDM cosmological model with $H_0 = 67.4\,\mathrm{km\,s^{-1}\,Mpc^{-1}}$, $\Omega_m = 0.315$, and $\Omega_\Lambda = 0.685$ (Planck Collaboration et al. 2020). This is also used to infer cosmological parameters such as the luminosity distance to GS-z14 and age of the Universe with the `Astropy` software package (Astropy Collaboration et al. 2013).

2. Observations

GS-z14 was first identified by K. N. Hainline et al. (2024b) with a photometric redshift $z_{\rm phot} = 14.51$, refined to $z_{\rm phot} = 14.39$ in the high-redshift galaxy population study by B. Robertson et al. (2024). Multiband JWST/NIRCam imaging was obtained as part of the JWST Advanced Deep Extragalactic Survey (JADES; D. J. Eisenstein et al. 2023a, Prog. IDs 1180 and 1210), the First Reionization Epoch Spectroscopically Complete Observations (P. A. Oesch et al. 2023, Prog. ID 1895), and of the JADES Origins Field (D. J. Eisenstein et al. 2023b; Prog. ID 3215). The data reduction is outlined in M. J. Rieke et al. (2023) and D. J. Eisenstein et al. (2023a, 2023b). The photometry implicitly used in this Letter (to scale the spectrum) was obtained by modeling the galaxy with a Sérsic profile, using the `forcepho` tool (B. Johnson 2025, in preparation), as described in S. Carniani et al. (2024). The distinctive advantage of `forcepho` is the ability to model the galaxy surface brightness before combining individual frames into a mosaic (e.g., W. M. Baker et al. 2025). The fiducial `forcepho` model yields a half-light semimajor axis of $R_{\rm UV} = 0.26$ kpc and a Sérsic index of 1. The gravitational lensing magnification from a foreground nearby galaxy at $z = 3.47$ is estimated to be only $\mu = 1.17$ (S. Carniani et al. 2024), so the lensing correction of 8% is smaller than the 10% systematic uncertainties of typical size measurements. GS-z14 has further been detected in 7.7 μm imaging with JWST/MIRI (J. M. Helton et al. 2025), implying the presence of strong nebular emission lines.

The JWST spectrum was first presented in S. Carniani et al. (2024). The data were obtained using the NIRSpec (P. Jakobsen et al. 2022) Micro-Shutter Assembly (P. Ferruit et al. 2022) with three-shutter slitlets (Prog. ID 1287, PI: Luetzgendorf). Here we focus on the prism spectrum,[10] which covers wavelengths $\lambda = 0.6$–$5.3\,\mu$m with a spectral resolving power $\mathcal{R} = 30$–300, although the most important spectral region in this Letter, the Lyα break at $\lambda \approx 2\,\mu$m, has $\mathcal{R} \sim 60$. The prism observations used the NRSIRS2 readout mode to mitigate pink noise (S. H. Moseley et al. 2010; B. J. Rauscher et al. 2017), with 19 groups per integration and 2 integrations per exposure, with three nodded exposures for accurate background subtraction. This sequence (about 2.33 hr total integration) was repeated four times, for a final on-source time of 9.3 hr. Following S. Carniani et al. (2024), we apply a flux correction factor to the reduced spectrum to match the normalization of the `forcepho` photometry data using a simple polynomial $F_{\rm corr} = F_{\rm red} \times (0.18 \times \lambda(\mu{\rm m}) + 1)$. This effectively takes into account and corrects for potential slit losses and/or uncertainties in the overall flux calibration.

Throughout this work, we adopt the spectral and physical galaxy measurements reported in S. Carniani et al. (2025). These were obtained using the `prospector` spectral-energy distribution (SED) modeling tool (B. D. Johnson et al. 2021), taking into account the full multiwavelength spectroscopic and imaging data obtained for GS-z14. This yields a star formation rate (SFR) $= 14.5 \pm 3\,M_\odot\,{\rm yr^{-1}}$ and a stellar mass of $\log(M_\star/M_\odot) = 8.29^{+0.09}_{-0.10}$, assuming a G. Chabrier (2003) initial mass function (IMF).

Dedicated far-infrared follow-up observations with ALMA were carried out to search for the [O III]-88 μm (Prog. ID: 2023.A.00037.S, PI: Schouws) and the [C II]-158μm (Prog. ID: 2024.A.00007.S, PI: Schouws) line transitions. [O III]-88 μm is detected at $>6\sigma$ with a line luminosity $L_{\rm [OIII]} = (2.0 \pm 0.5) \times 10^8\,L_\odot$ (S. Carniani et al. 2025; S. Schouws et al. 2024). Deep ALMA observations targeting the [C II]-158 μm line, however, resulted in a nondetection at a limit $<6 \times 10^7\,L_\odot$ (3σ; S. Schouws et al. 2025), though still consistent with the typical high-redshift galaxy population (S. Carniani et al. 2020; Y. Harikane et al. 2020). Here we examine the constraints delivered from the far-infrared line transitions in context of the H I column density and physical properties to probe the full baryonic matter budget of GS-z14.

3. Analysis and Results

Based on the observed Lyα break, and given the lack of strong rest-frame UV/optical nebular emission lines, S. Carniani et al. (2024) inferred a redshift of $z_{\rm Ly\alpha,break} = 14.32^{+0.08}_{-0.20}$, with the large uncertainties due to the covariance between redshift and H I column density. The significant detection of the far-infrared [O III]-88 μm emission line reveals the systemic redshift to be $z = 14.1796 \pm 0.0006$ (S. Carniani et al. 2025; S. Schouws et al. 2024). This measurement can break the degeneracy between redshift and H I column density and constrains that a substantial H I column density arising in proximate neutral gas has imprinted a pronounced Lyα damping-wing absorption profile on the rest-frame UV

[10] Available on Zenodo at DOI:10.5281/zenodo.12578542 (see S. Carniani 2024).

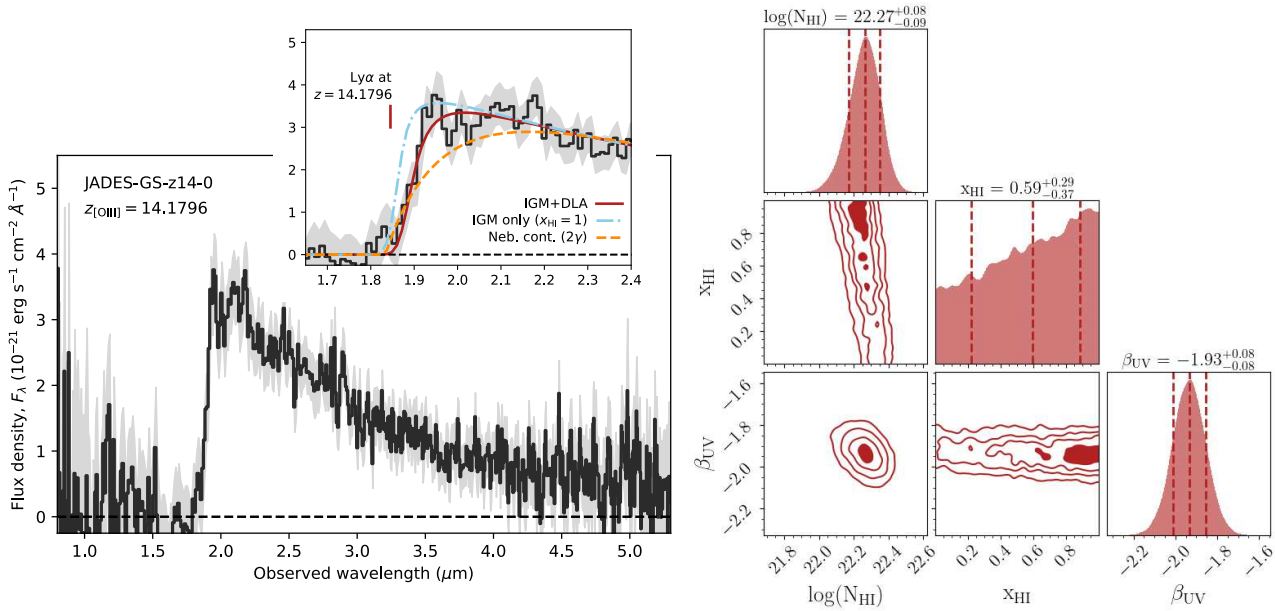

Figure 1. (Left) JWST/NIRSpec Prism 1D spectrum of GS-z14. The photometrically corrected flux density is shown by the black curve, and the associated uncertainty is shown by the gray shaded region. In the inset is shown a zoom-in on the rest-frame UV part of the spectrum, with the best-fit DLA model overplotted (red solid curve), an IGM-only model (blue dotted–dashed), and predictions for a 2γ nebular continuum emission (orange dashed line). (Right) Corner plot of the posterior distributions from the spectroscopic modeling, with the median and 16–84 percentiles marked.

continuum (S. Carniani et al. 2025). We assume that [O III]-88 μm traces the overall star-forming region of the galaxy and use that as the systemic redshift, and we find that the DLA redshift is consistent with this (within the spectral resolution of the data). We model the DLA absorption with a Voigt profile following K. E. Heintz et al. (2024a; see also C. L. Pollock et al. 2025, in preparation), using the approximation from T. Tepper-García (2006) and convolve the best-fit model with the spectral resolution at each step during the optimization. The high H I column densities of the absorbing gas effectively make this modeling only sensitive to the H I column density, N_{HI}, reflected in the broad, prominent Lyα damping wing. Still, we include the unconstrained x_{HI} to fully capture the covariance between this and the other two parameters in the model. We assume that the rest-frame UV continuum can be approximated by a smooth power-law function, $F_\lambda \propto \lambda^{-\beta_{UV}}$. Introducing more complex spectral shapes or prominent Lyα emission does not significantly affect the derived N_{HI} (K. E. Heintz et al. 2024b), at least at high H I column densities (M. Huberty et al. 2025). We also include a prescription of the neutral hydrogen fraction $x_{HI} = n_{HI}/n_{H,tot}$ of the IGM on our modeling, which we expect to be fully neutral at $z \approx 14$ (J. Miralda-Escudé 1998; A. K. Inoue et al. 2014). We use `dynesty` nested sampling (J. S. Speagle 2020) to sample the posteriors of the parameters $\log(N_{HI})$, x_{HI}, and β_{UV}, assuming a fixed DLA redshift of $z = 14.1796$.

The best-fit DLA model is shown in Figure 1, together with the posterior distributions on the derived quantities: $\log(N_{HI}/\mathrm{cm}^{-2}) = 22.27^{+0.08}_{-0.09}$, $x_{HI} > 0.41$ (1σ from the 68% highest density interval), and $\beta_{UV} = -1.93 \pm 0.08$. The derived N_{HI} is 0.3 dex higher than the column density inferred from the full spectrophotometric fitting by S. Carniani et al. (2024), though still consistent within 3σ. Setting the neutral hydrogen fraction to $x_{HI} = 1$ as expected at $z = 14$ does not significantly change the result since the DLA from the local H I gas dominates the optical depth of the Lyα absorption profile. Considering a model with only an IGM contribution ($x_{HI} = 1$) provides a statistically worse fit to the data with $\chi^2_\nu = 1.69$, compared to $\chi^2_\nu = 1.23$ for the fit with a DLA component. Additionally, the difference in Bayesian information criteria between the models $\Delta \mathrm{BIC} = 82$ indicates a strong statistical preference for the IGM+DLA model (see Figure 1). We also compare the DLA model to a purely nebular continuum model, dominated by the two-photon (2γ) emission at rest-frame UV wavelengths, assuming $T = 20{,}000$ K and $n_e = 10^2\,\mathrm{cm}^{-3}$ from M. Schirmer (2016). This matches well the slope of the spectrum, but the strong UV turnover is inconsistent with the data ($\chi^2_\nu = 1.53$). With an absolute UV magnitude, $M_{UV} = -20.81 \pm 0.16$ mag (S. Carniani et al. 2024), GS-z14 is thus an exemplary case of a bright, star-forming galaxy embedded in a substantial neutral gas reservoir.

To gauge the total H I gas mass of the galaxy, we use the measured H I column density in the line of sight and assume that the half-mass–radius of the neutral gas is $\sim 3\times$ the rest-frame UV size (consistent with constraints of $z \sim 6$ galaxies from ALMA; S. Fujimoto et al. 2020; Y. Fudamoto et al. 2022). For a spherically distributed gas, this yields an H I gas mass of $M_{HI} = 5 \times 10^9\,M_\odot$, substantially higher than the previously reported upper bound inferred on the (molecular) gas mass, $M_{mol} < 10^{9.2}\,M_\odot$ (S. Schouws et al. 2025). If we consider the metallicity-dependent relation converting the [C II]-158 μm line luminosity into a H I gas mass (K. E. Heintz et al. 2021), based on γ-ray burst sightlines through high-redshift star-forming galaxies, we derive an upper bound of $M_{HI} < 10^{9.9}\,M_\odot$ (3σ). This suggests that the derived H I gas masses are still consistent within the upper bound allowed by the nondetection of the [C II]-158 μm emission, taking into account the relatively low metallicity of the galaxy. However, this estimate of M_{HI} from the DLA N_{HI} is heavily dependent on the assumed geometry of the system. To corroborate the evidence for a substantial gas fraction in the system, we

consider the Kennicutt–Schmidt relation (R. C. Kennicutt & N. J. Evans 2012), universally connecting the SFR and gas surface density. We determine the SFR surface density as $\Sigma_{\rm SFR} = {\rm SFR}_{\rm UV}/2\pi R_{\rm UV}^2$, which given the half-light radius $R_{\rm UV} = 0.26$ kpc reported by S. Carniani et al. (2024) yields $\log(\Sigma_{\rm SFR}/M_\odot\ {\rm yr}^{-1}\,{\rm kpc}^{-2}) = 1.5 \pm 0.30$ (assuming an inflated 30% error on the SFR). This implies a molecular gas surface density of $\log(\Sigma_{\rm H_2}/M_\odot\ {\rm pc}^{-2}) = 3.6 \pm 0.3$ following the global galaxy Kennicutt–Schmidt relation, which we convert to a molecular gas mass of $\log(M_{\rm H_2}/M_\odot) = 9.2 \pm 0.3$ within the star-forming region, at the limit for the upper bound derived from the [C II]-to-H_2 conversion (S. Schouws et al. 2025). The global Kennicutt–Schmidt relation for the total (H I + H_2) gas mass predicts a higher total gas surface density $\log(\Sigma_{\rm gas}/M_\odot\ {\rm pc}^{-2}) = 4.2 \pm 0.3$ and total gas mass $\log(M_{\rm gas}/M_\odot) = 9.8 \pm 0.3$ within the star-forming region. Taken at face value, this implies a large gas fraction $f_{\rm gas} = M_{\rm gas}/(M_\star + M_{\rm gas}) \gtrsim 0.9$. Further, this estimate is consistent with the bulk of the interstellar medium (ISM) in GS-z14 being in the form of H I ($M_{\rm HI} = M_{\rm gas} - M_{\rm H_2} = 5 \times 10^9\,M_\odot$, such that the inferred atomic-to-molecular gas mass ratio is $M_{\rm HI} \approx 3 \times M_{\rm H_2}$), exactly as predicted from the DLA H I column density.

Alternatively, we can determine the metal mass of GS-z14 from the measured line detection of [O III]-88 μm and convert into a gas mass based on the metallicity quantified as an oxygen abundance, $\log({\rm O/H}) = 7.92$ (for $Z/Z_\odot = 0.17$ and a solar oxygen abundance of $12 + \log({\rm O/H})_\odot = 8.69$; M. Asplund et al. 2009). The metal mass in the ISM is defined as $M_Z = M_{\rm gas} \times Z/Z_\odot \times Z_{\odot,{\rm ref}}$ with $Z_{\odot,{\rm ref}} = 0.018$. Using the set of observations from the local *Herschel* dwarf galaxy survey (D. Cormier et al. 2015) and smoothed particle hydrodynamics simulations applied to cosmological zoom-in simulations (K. Olsen et al. 2017), we find that the [O III]-to-M_Z calibration is anticorrelated with the $L_{\rm [OIII]}/L_{\rm [CII]}$ line luminosity ratio (see also K. E. Heintz et al. 2023c), such that $\log(M_Z/L_{\rm [OIII]}) = -1.0 \pm 0.2$ for $L_{\rm [OIII]}/L_{\rm [CII]} > 3$. This yields a total metal mass in the ISM of $M_Z = (2.0 \pm 0.6) \times 10^7\,M_\odot$, which implies a total gas mass of $\sim 10^{9.8}\,M_\odot$ when taking the metallicity of GS-z14 into account, consistent with the above estimates.

To investigate in more detail the composition of the absorbing gas, we determine the dust-to-gas ratio, $A_V/N_{\rm HI}$. Here, $N_{\rm HI}$ is derived from the DLA model, and the visual extinction A_V is determined from the spectral slope. Assuming a steep, intrinsic power law with $\beta_{\rm UV} = -3$ requires $A_V = 0.3$ mag for a Small Magellanic Cloud–like reddening curve (K. D. Gordon et al. 2003) to match the observed rest-frame UV spectral slope. This quantity is effectively the maximum-allowed amount of dust in the line of sight that will extinguish the light, since the intrinsic spectral slope will be redder for a slightly older stellar population on average. This upper bound is also consistent with the visual attenuation $A_V = 0.25 \pm 0.10$ inferred from the full spectrophotometric modeling of the SED and line emission for GS-z14 (S. Carniani et al. 2025; which we assume in the following). This yields a dust-to-gas ratio of $A_V/N_{\rm HI} = (1.3 \pm 0.6) \times 10^{-23}$ mag cm^2. We compare this to equivalent measures from the compilation of γ-ray burst sightlines through high-redshift ($z = 1.7$–6.3) star-forming galaxies presented in K. E. Heintz et al. (2023a) and to the average value observed in the Milky Way and the Small and Large Magellanic Clouds (C. Konstantopoulou et al. 2024) in Figure 2. The local galaxy and GRB sightlines show a consistent increase in the dust-to-gas ratio with metallicity, independent of redshift. In contrast, it is evident that GS-z14 has a comparably lower dust-to-gas ratio given its derived metallicity, consistent with the most metal-poor ([M/H]< -1.0) γ-ray burst sightlines. This suggests that this particular sightline either has a low dust-to-gas ratio due to inefficient dust production (or more violent dust destruction mechanisms) or that the DLA mainly traces more pristine gas than the galaxy itself. The empirical, best-fit relation indicate a gas-phase metallicity of $-1.90 < {\rm [M/H]} < -1.15$ (or $12 + \log({\rm O/H}) = 6.75-7.55$). The inferred lower gas-phase metallicity from this approach compared to the emission-line metallicity is similar in methodology and consistent with the results from F. D'Eugenio et al. (2024) for GS-z12 at $z = 12.5$. We will discuss the observed dust deficit further in Section 4 below.

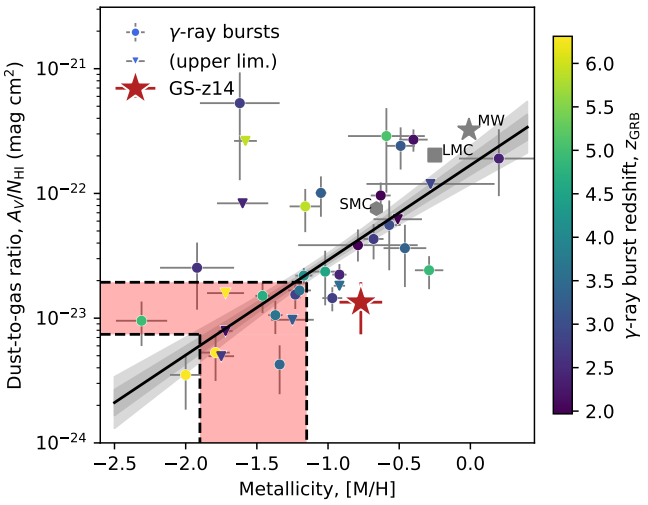

Figure 2. Dust-to-gas ratio, $A_V/N_{\rm HI}$, as a function of gas-phase metallicity, [M/H]. GS-z14 is shown by the red star symbol and the high-redshift γ-ray burst sightlines through star-forming galaxies at $z = 1.7$–6.3 as the colored circles (measurements) or triangles (upper limits). The best-fit relation for the γ-ray burst sample is shown by the black solid line, with the 1σ and 2σ uncertainty indicated by the dark- and light-gray shaded region. The red shaded region marks the expected gas-phase metallicity from the relation, assuming the measured dust-to-gas ratio of GS-z14, $A_V/N_{\rm HI} = (1.3 \pm 0.6) \times 10^{-23}$ mag cm^2.

4. Discussion and Conclusions

We have examined in detail the gas content of the most distant, spectroscopically confirmed galaxy observed to date, GS-z14 at $z = 14.179$ (S. Carniani et al. 2024, 2025; S. Schouws et al. 2024). This galaxy is relatively bright, with an absolute UV magnitude $M_{\rm UV} = -20.8$ mag, a stellar mass $M_\star \sim 10^{8.3}\,M_\odot$, and shows evidence for chemically enriched gas ($Z/Z_\odot \sim 0.17$). We determined the total H I column density for GS-z14 to be $\log(N_{\rm HI}/{\rm cm}^2) = 22.27^{+0.08}_{-0.09}$, integrated over the line of sight. Assuming a simple spherical geometry, this implies a substantial H I gas mass of $M_{\rm HI} = 5 \times 10^9\,M_\odot$. While a spherical geometry is an oversimplification, the high detection rate of DLA around galaxies at $z > 10$ (K. E. Heintz et al. 2025) almost certainly implies a high covering factor, closer to a spherical distribution than to a thin disk. Importantly, we found this large H I gas mass estimate to be consistent with the expected total gas mass from the SFR surface density and the universal Kennicutt–

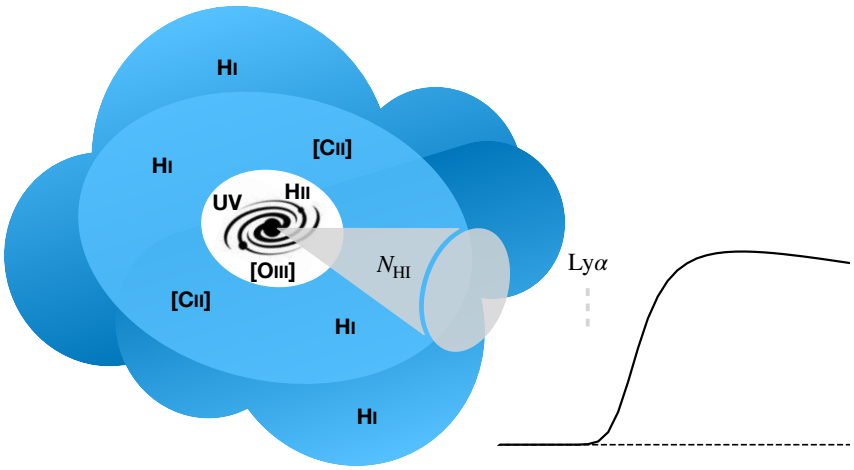

Figure 3. Schematic of the gas components seen in absorption and emission for GS-z14. The central star-forming H II regions also emit most of the rest-frame UV and [O III] emission. The more extended neutral gas region likely dominates the observed H I column density and more diffuse [C II] emission due to the lower metallicity of the gas. The compact size of the young stellar population increases the ionization parameter U and the [O III]/[C II] line ratio. Inspired by Y. Harikane et al. (2020).

Schmidt relation and within the limits allowed by the nondetection of the [C II]-158 μm line emission (S. Schouws et al. 2025). These independent but complementary measurements all pointed to a total gas mass of the order $\log(M_{\rm gas}/M_{\odot}) = 9.8 \pm 0.3$, implying a substantial gas mass fraction, $f_{\rm gas} \gtrsim 0.9$. Assuming a bottom-light or top-heavy IMF (e.g., M. R. Bate 2023, 2025; H. Katz et al. 2024) would increase the fraction even further. This implies that the bulk ISM, and the baryonic matter content of GS-z14 overall, is largely dominated by H I. Based on the low visual attenuation, $A_V = 0.25 \pm 0.10$ mag, we determined that the metallicity of the DLA is lower than that of the central star-forming region. This suggested that GS-z14 is embedded in a substantial, pristine neutral gas reservoir.

Previous estimates reporting a low gas fraction, $f_{\rm gas} \lesssim 0.7$, for GS-z14 are based on the dynamical mass estimated within the [O III]-88 μm emitting region ($\log(M_{\rm dyn}/M_{\odot}) = 9.0 \pm 0.2$) and the nondetection of the [C II]-158 μm emission line (S. Carniani et al. 2025; S. Schouws et al. 2025). We argue that since [O III]-88 μm solely originates from the central, most intense star-forming regions (as is also the case for C III] λ1909), this line transition is arguably not a reliable tracer of the total baryonic matter in the galaxy. Indeed, the rest-frame UV and the [O III]-88 μm emission has been observed to be much more spatially compact than the [C II]-158 μm emitting region (e.g., S. Fujimoto et al. 2020; Y. Harikane et al. 2020; R. Herrera-Camus et al. 2021; Y. Fudamoto et al. 2022). The fact that it is consistent with the inferred stellar mass from the SED modeling (S. Carniani et al. 2025) instead supports this line mostly tracing the central star-forming component. The upper bound on the molecular gas mass inferred from the nondetection of [C II]-158 μm (S. Schouws et al. 2025) will also likely underestimate the total gas mass of the galaxy, given that [C II] predominantly traces the neutral atomic gas, in particular in low-metallicity regions (K. E. Heintz et al. 2022; S. C. Madden et al. 1993). This is because the ionization potential of neutral carbon (11.26 eV) is below that of neutral hydrogen (13.6 eV), such that any inherent ISM radiation field will ionize carbon to C^+ in the neutral ISM. Indeed, the substantial H I column density suggest that there is a large abundance of neutral H outside the central H II region. We show a schematic of this proposed interpretation in Figure 3. We note that the H_2 fraction may be suppressed in these galaxies by the lack of dust compared to lower-redshift galaxies and that the lack of [C II] could also be explained by a low C/O abundance ratio (S. Carniani et al. 2025), which is expected for low-metallicity galaxies (e.g., D. C. Nicholls et al. 2017; K. Z. Arellano-Córdova et al. 2022; T. Jones et al. 2023; M. Curti et al. 2025), or the high ionization parameter $\log U = -2.4$, which suppresses [C II] in favor of C III].

The analytical model developed for GS-z14 by A. Ferrara (2024) of its star formation history and general physical properties is generally consistent with the observed quantities (S. Carniani et al. 2025) and particularly predicts a low dust-to-gas mass ratio of $10^{-3.5}$. This is exactly at the limit we predict from the total gas mass and the upper bound on the dust mass $<10^6\,M_{\odot}$ from the far-infrared continuum (S. Schouws et al. 2024). We note that the observed dust-to-gas mass ratio ($<10^{-3.5}$) is $\sim$10$\times$ lower than the Galactic average (C. Konstantopoulou et al. 2024) but consistent with the general trend seen at the local to high-redshift universe considering its low metallicity (K. E. Heintz et al. 2023a). Further, the line-of-sight dust-to-gas ratio, $A_V/N_{\rm HI}$, is equally lower than the Galactic average at 4.5×10^{-22} mag cm^2 (D. Watson 2011). These independent measures thus validate the low dust content of GS-z14 but suggest that it is primarily driven by the metallicity of the galaxy.

Our results have important implications for the follow-up strategies with both JWST and ALMA for characterizing in depth the gas and metal abundances of very high-redshift ($z > 10$) galaxies. First, the typical lower metallicities of the galaxies affect the C/O abundance ratio and how in particular the far-infrared [C II]-158 μm emission scales with the neutral gas mass (H. Katz et al. 2022), while the [O III]-88 μm transition remains a valid tracer of the star formation activity of even the most distant galaxies. This greatly motivates targeting the [O III]-88 μm line transition (e.g., R. J. Bouwens et al. 2022) to accurately pinpoint the redshift of very high-redshift galaxies. We caution, however, that the gas mass

inferred from the dynamics of [O III] will likely underestimate the true total baryonic matter content of the sources. Second, the typical strong DLAs detected in the spectra of galaxies at $z > 10$ (K. E. Heintz et al. 2024b, 2025; H. Umeda et al. 2023; Y. Asada et al. 2025; F. D'Eugenio et al. 2024; K. N. Hainline et al. 2024a; J. Witstok et al. 2025) need to be taken into account when designing the far-infrared line scan configuration, which will be at a lower redshift than implied from the Lyα break alone. Finally, quantifying the metal abundance in the absorbing gas traced by the DLA will help disentangle whether this is mainly pristine, intergalactic gas or consistent with the chemically enriched interstellar inferred from the SED and nebular emission-line ratios. For the substantial H I column densities $N_{\rm HI} \gtrsim 10^{22}\,{\rm cm}^{-2}$ and metallicities $Z/Z_{\odot} \sim 10\%$ seen in GS-z14 and other spectroscopically confirmed galaxies at $z > 10$, we would expect to be able to detect the low-ion metal absorption lines from O I λ1302 or C II λ1334, tracing the metal abundance of the neutral gas, in the higher resolution JWST/NIRSpec grating spectra. The main challenge will be to achieve high-enough signal to noise in the rest-frame UV continuum to robustly measure the optical depth and thereby the column densities of the metal absorption lines, which requires substantial exposure times even for the intrinsically bright GS-z14 due to the large cosmological distances. This measure will, however, definitely establish whether the massive DLAs seen in most high-redshift spectra are predominantly tracing primordial or chemically enriched neutral atomic gas at cosmic dawn.

Acknowledgments

We would like to thank Johan Fynbo and Peter Laursen for the insightful discussions about the interpretation of the results presented in this work. We also acknowledge and appreciate the substantial amount of work from the JADES collaboration in defining and carrying out the JWST/NIRSpec spectroscopic follow-up of the most distant galaxies uncovered to date. This work has received funding from the Swiss State Secretariat for Education, Research and Innovation (SERI) under contract number MB22.00072. The Cosmic Dawn Center (DAWN) is funded by the Danish National Research Foundation under grant DNRF140. FDE acknowledges the ERC Advanced Grant 695671 "QUENCH" and support by the Science and Technology Facilities Council (STFC) and by the UKRI Frontier Research grant RISEandFALL.

This work is based on observations made with the NASA/ESA/CSA James Webb Space Telescope. The data were obtained from the Mikulski Archive for Space Telescopes at the Space Telescope Science Institute, which is operated by the Association of Universities for Research in Astronomy, Inc., under NASA contract NAS 5-03127 for JWST. These observations are associated with programs #1210, #1287, and #3215. The specific data used can be accessed on Zenodo DOI:10.5281/zenodo.12578542. This work was furthermore based on observations taken by the Atacama Large Millimeter/submillimeter Array (ALMA). ALMA is a partnership of ESO (representing its member states), NSF (USA), and NINS (Japan), together with NRC (Canada), MOST and ASIAA (Taiwan), and KASI (Republic of Korea), in cooperation with the Republic of Chile. The Joint ALMA Observatory is operated by ESO, AUI/NRAO, and NAOJ.

Facilities: JWST (NIRSpec), ALMA.

Software: Astropy (Astropy Collaboration et al. 2013), Matplotlib (J. D. Hunter 2007), NumPy (C. R. Harris et al. 2020).

ORCID iDs

Kasper E. Heintz https://orcid.org/0000-0002-9389-7413
Clara L. Pollock https://orcid.org/0009-0001-2808-4918
Joris Witstok https://orcid.org/0000-0002-7595-121X
Stefano Carniani https://orcid.org/0000-0002-6719-380X
Kevin N. Hainline https://orcid.org/0000-0003-4565-8239
Francesco D'Eugenio https://orcid.org/0000-0003-2388-8172
Chamilla Terp https://orcid.org/0009-0005-4175-4890
Darach Watson https://orcid.org/0000-0002-4465-8264

References

Algera, H., Rowland, L., Stefanon, M., et al. 2025, arXiv:2501.10508
Aravena, M., Heintz, K., Dessauges-Zavadsky, M., et al. 2024, A&A, 682, A24
Arellano-Córdova, K. Z., Berg, D. A., Chisholm, J., et al. 2022, ApJL, 940, L23
Arrabal Haro, P., Dickinson, M., Finkelstein, S. L., et al. 2023, Natur, 622, 707
Asada, Y., Desprez, G., Willott, C. J., et al. 2025, ApJ, 983, L2
Asplund, M., Grevesse, N., Sauval, A. J., & Scott, P. 2009, ARA&A, 47, 481
Astropy Collaboration, Robitaille, T. P., Tollerud, E. J., et al. 2013, A&A, 558, A33
Atek, H., Shuntov, M., Furtak, L. J., et al. 2023, MNRAS, 519, 1201
Austin, D., Conselice, C. J., Adams, N. J., et al. 2024, arXiv:2404.10751
Baker, W. M., Tacchella, S., Johnson, B. D., et al. 2025, NatAs, 9, 141
Bate, M. R. 2023, MNRAS, 519, 688
Bate, M. R. 2025, MNRAS, 537, 752
Bouwens, R. J., Smit, R., Schouws, S., et al. 2022, ApJ, 931, 160
Bouwens, R. J., Stefanon, M., Brammer, G., et al. 2023, MNRAS, 523, 1036
Bunker, A. J., Saxena, A., Cameron, A. J., et al. 2023, A&A, 677, A88
Carniani, S. 2024, The Spectroscopic Confirmation of Two Luminous Galaxies at z ~ 14, v1, Zenodo, doi:10.5281/zenodo.12578542
Carniani, S., D'Eugenio, F., Ji, X., et al. 2025, A&A, 696, A87
Carniani, S., Ferrara, A., Maiolino, R., et al. 2020, MNRAS, 499, 5136
Carniani, S., Hainline, K., D'Eugenio, F., et al. 2024, Natur, 633, 318
Castellano, M., Fontana, A., Treu, T., et al. 2022, ApJL, 938, L15
Castellano, M., Fontana, A., Treu, T., et al. 2023, ApJL, 948, L14
Castellano, M., Napolitano, L., Fontana, A., et al. 2024, ApJ, 972, 143
Chabrier, G. 2003, PASP, 115, 763
Cormier, D., Madden, S. C., Lebouteiller, V., et al. 2015, A&A, 578, A53
Curti, M., Witstok, J., Jakobsen, P., et al. 2025, A&A, 697, A89
Curtis-Lake, E., Carniani, S., Cameron, A., et al. 2023, NatAs, 7, 622
D'Eugenio, F., Maiolino, R., Carniani, S., et al. 2024, A&A, 689, A152
Donnan, C. T., McLeod, D. J., Dunlop, J. S., et al. 2023, MNRAS, 518, 6011
Eisenstein, D. J., Johnson, B. D., Robertson, B., et al. 2023b, arXiv:2310.12340
Eisenstein, D. J., Willott, C., Alberts, S., et al. 2023a, arXiv:2306.02465
Ferrara, A. 2024, A&A, 689, A310
Ferruit, P., Jakobsen, P., Giardino, G., et al. 2022, A&A, 661, A81
Finkelstein, S. L., Leung, G. C. K., Bagley, M. B., et al. 2024, ApJL, 969, L2
Fudamoto, Y., Smit, R., Bowler, R. A. A., et al. 2022, ApJ, 934, 144
Fujimoto, S., Arrabal Haro, P., Dickinson, M., et al. 2023a, ApJL, 949, L25
Fujimoto, S., Finkelstein, S. L., Burgarella, D., et al. 2023b, ApJ, 955, 130
Fujimoto, S., Silverman, J. D., Bethermin, M., et al. 2020, ApJ, 900, 1
Gordon, K. D., Clayton, G. C., Misselt, K. A., Landolt, A. U., & Wolff, M. J. 2003, ApJ, 594, 279
Hainline, K. N., D'Eugenio, F., Jakobsen, P., et al. 2024a, ApJ, 976, 160
Hainline, K. N., Johnson, B. D., Robertson, B., et al. 2024b, ApJ, 964, 71
Harikane, Y., Ouchi, M., Inoue, A. K., et al. 2020, ApJ, 896, 93
Harikane, Y., Ouchi, M., Oguri, M., et al. 2023, ApJS, 265, 5
Harris, C. R., Millman, K. J., van der Walt, S. J., et al. 2020, Natur, 585, 357
Heintz, K. E., Bennett, J. S., Oesch, P. A., et al. 2024a, arXiv:2407.06287
Heintz, K. E., Brammer, G. B., Watson, D., et al. 2025, A&A, 693, A60
Heintz, K. E., De Cia, A., Thöne, C. C., et al. 2023a, A&A, 679, A91
Heintz, K. E., Giménez-Arteaga, C., Fujimoto, S., et al. 2023b, ApJL, 944, L30
Heintz, K. E., Oesch, P. A., Aravena, M., et al. 2022, ApJL, 934, L27

Heintz, K. E., Shapley, A. E., Sanders, R. L., et al. 2023c, A&A, 678, A30
Heintz, K. E., Watson, D., Brammer, G., et al. 2024b, Sci, 384, 890
Heintz, K. E., Watson, D., Oesch, P. A., Narayanan, D., & Madden, S. C. 2021, ApJ, 922, 147
Helton, J. M., Rieke, G. H., Alberts, S., et al. 2025, NatAs, 9, 729
Herrera-Camus, R., Förster Schreiber, N., Genzel, R., et al. 2021, A&A, 649, A31
Hsiao, T. Y.-Y., Abdurro'uf, Coe, D., et al. 2024a, ApJ, 973, 8
Hsiao, T. Y.-Y., Álvarez-Márquez, J., Coe, D., et al. 2024b, ApJ, 973, 81
Huberty, M., Scarlata, C., Hayes, M. J., & Gazagnes, S. 2025, arXiv:2501.13899
Hunter, J. D. 2007, CSE, 9, 90
Inoue, A. K., Shimizu, I., Iwata, I., & Tanaka, M. 2014, MNRAS, 442, 1805
Jakobsen, P., Ferruit, P., Alves de Oliveira, C., et al. 2022, A&A, 661, A80
Johnson, B. D., Leja, J., Conroy, C., & Speagle, J. S. 2021, ApJS, 254, 22
Jones, T., Sanders, R., Chen, Y., et al. 2023, ApJL, 951, L17
Katz, H., Cameron, A. J., Saxena, A., et al. 2024, arXiv:2408.03189
Katz, H., Rosdahl, J., Kimm, T., et al. 2022, MNRAS, 510, 5603
Kennicutt, R. C., & Evans, N. J. 2012, ARA&A, 50, 531
Kokorev, V., Atek, H., Chisholm, J., et al. 2025, ApJL, 983, L22
Konstantopoulou, C., De Cia, A., Ledoux, C., et al. 2024, A&A, 681, A64
Madden, S. C., Geis, N., Genzel, R., et al. 1993, ApJ, 407, 579
Miralda-Escudé, J. 1998, ApJ, 501, 15
Moseley, S. H., Arendt, R. G., Fixsen, D. J., et al. 2010, Proc. SPIE, 7742, 77421B
Naidu, R. P., Oesch, P. A., Setton, D. J., et al. 2022, arXiv:2208.02794
Nicholls, D. C., Sutherland, R. S., Dopita, M. A., Kewley, L. J., & Groves, B. A. 2017, MNRAS, 466, 4403
Oesch, P. A., Brammer, G., Naidu, R. P., et al. 2023, MNRAS, 525, 2864
Olsen, K., Greve, T. R., Narayanan, D., et al. 2017, ApJ, 846, 105
Planck Collaboration, Aghanim, N., Akrami, Y., et al. 2020, A&A, 641, A6
Rauscher, B. J., Arendt, R. G., Fixsen, D. J., et al. 2017, PASP, 129, 105003
Rieke, M. J., Robertson, B., Tacchella, S., et al. 2023, ApJS, 269, 16
Robertson, B., Johnson, B. D., Tacchella, S., et al. 2024, ApJ, 970, 31
Robertson, B. E. 2022, ARA&A, 60, 121
Schirmer, M. 2016, PASP, 128, 114001
Schouws, S., Bouwens, R. J., Algera, H., et al. 2025, arXiv:2502.01610
Schouws, S., Bouwens, R. J., Ormerod, K., et al. 2024, arXiv:2409.20549
Speagle, J. S. 2020, MNRAS, 493, 3132
Tepper-García, T. 2006, MNRAS, 369, 2025
Umeda, H., Ouchi, M., Nakajima, K., et al. 2023, arXiv:2306.00487
Watson, D. 2011, A&A, 533, A16
Witstok, J., Jakobsen, P., Maiolino, R., et al. 2025, Natur, 639, 897
Whitler, L., Stark, D. P., Topping, M. W., et al. 2025, arXiv:2501.00984
Zavala, J. A., Bakx, T., Mitsuhashi, I., et al. 2024, ApJL, 977, L9
Zavala, J. A., Castellano, M., Akins, H. B., et al. 2025, NatAs, 9, 155